AIAA JOURNAL
Vol. 46, No. 10, October 2008

Skin-Friction Measurements Using Oil-Film Interferometry in NASA's 11-Foot Transonic Wind Tunnel

David M. Driver*
NASA Ames Research Center, Moffett Field, California 94035
and
Aaron Drake†
Northrop Grumman Corporation, El Segundo, California 90245

DOI: 10.2514/1.7570

Skin-friction measurements were obtained on two laminar flow airfoils in the NASA Ames 11-ft transonic wind tunnel using oil-film interferometry. Improvements in the experimental technique allowed skin-friction measurements at two conditions per run in conjunction with performance testing, thus reducing the impact on the run schedule. Quantitative measurements of skin friction were used to determine transition location and the extent of separation (if any) on the airfoils providing much more insight into the flow than flow viz. The technique has been extended to obtain a quantitative measure of shear in the reversed flow region. The effects of various disturbances to the boundary layer were also investigated. Laminar flow was found as far back as 60% chord at a Reynolds number of 4.5×10^6.

Introduction

OIL-FILM interferometry has become an increasingly popular way to make measurements of skin friction in large scale facilities [1–5]. The reason for this is due to the technique's relative ease of implementation and the solid theoretical underpinning that makes it a direct measure of shear rather than a correlation from which shear is inferred. The need for locating transition position is often a primary motivation for applying the technique.

Often, in large facilities, the desire to obtain skin-friction measurements and transition location is offset by the reluctance to dedicate time in the run schedule (typically 1 h per run). Consequently, although the use of oil-film interferometry is on the rise in research facilities, it has been used sparingly in production wind-tunnel tests.

In this paper we describe the way in which we have limited the impact on run schedule while at the same time acquiring high quality skin-friction measurements for two conditions per run. Measurements are obtained on a laminar flow airfoil in the NASA Ames 11-ft transonic wind tunnel. The technique was successfully applied in both the laminar and turbulent regions of the flow. Furthermore we describe a way to obtain skin-friction measurements in the reversed flow region when the fringes are contracting.

Oil-Film Interferometry

The oil-film interferometry technique was originally devised by Tanner and Blows [6] and subsequently modified to its current state by Monson et al. [7]. The technique works on the principle that oil applied to an aerodynamic surface will flow and thin due to shear (see Fig. 1). As time goes on the oil becomes thin to the point that interference patterns known as fringes (visible under illumination by monochromatic light) will be spaced far enough apart to be visible in the oil (see Fig. 2). The shear is then determined from a measurement of the oil's thinning rate and application of the thin film equations [8,9].

The spacing between the fringes Δs is related to skin friction by the equation of Monson et al. [7], which is derived from one-dimensional thin oil-film equations [3,8,9]

$$C_f = \frac{\tau_w}{q_\infty} = \frac{(2n_o/\lambda)\cos(\theta_r)(\Delta s)}{\int_{t_o}^{t}(q_\infty/\mu_o)\,\mathrm{d}t} \tag{1}$$

The numerator on the right-hand side of the equation is an interferometric measure of the reciprocal of the oil-film slope. Here n_o is the oil's index of refraction, θ_r is the refracted light angle through the oil, and λ is the wavelength of the light source illuminating the oil. The integral, containing the hydraulic quantities of the oil's viscosity μ_o and the tunnel dynamic pressure q_∞, is integrated over time t of the tunnel run where time t_o is a time before the tunnel is started. The light refraction angle through the oil is related to the angle of incidence of the light source $\theta_r = \sin^{-1}(\sin\theta_i/n_o)$.

The main assumptions in Eq. (1) are that the skin-friction coefficient (C_f) is constant over the entire duration of the run and that at time t_o, before the oil begins to flow, the oil is infinitely thick ($\Delta s = 0$). An intermediate step in the derivation [3,8,9] of Eq. (1) yields

$$C_f = \frac{\tau_w}{q_\infty} = \frac{(2n_o/\lambda)\cos(\theta_r)(\Delta s_{n+1} - \Delta s_n)}{\int_{t_n}^{t_{n+1}}(q_\infty/\mu_o)\,\mathrm{d}t} \tag{2}$$

This requires that the skin-friction coefficient be constant only during the time t_n through t_{n+1} and that the fringe spacing (Δs_n and Δs_{n+1}) be measured at these times. Equation (2) can also be derived from Eq. (1) by rewriting Eq. (1) in the form

$$C_f \int_{t_o}^{t_n}(q_\infty/\mu_o)\,\mathrm{d}t = \Delta s_n(2n_o/\lambda)\cos(\theta_r)$$

and again

$$C_f \int_{t_o}^{t_{n+1}}(q_\infty/\mu_o)\,\mathrm{d}t = \Delta s_{n+1}(2n_o/\lambda)\cos(\theta_r)$$

where t_n and t_{n+1} have been substituted for t in the two forms, respectively. By subtracting one equation from the other, the contribution of the integral

Presented as Paper 1359 at the 42nd AIAA Aerospace Sciences Meeting and Exhibit, Reno, Nevada, 5–8 January 2004; received 13 January 2004; accepted for publication 19 June 2006.

*David.M.Driver@nasa.gov. AIAA member.
†Aaron.Drake@ngc.com. AIAA member.

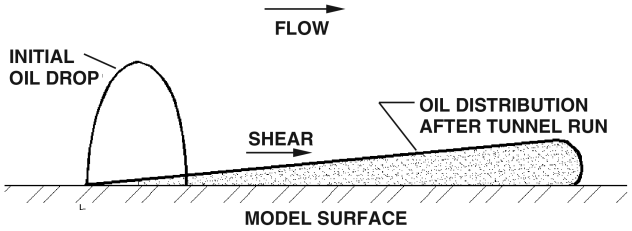

Fig. 1 Oil deposit before and after a tunnel run.

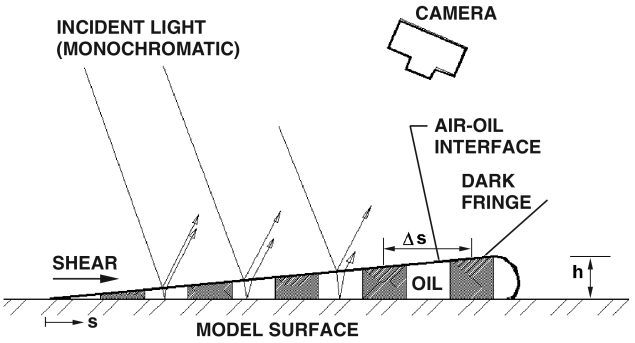

Fig. 2 Bands of dark and light (fringes) seen in an oil film as a result of interference.

$$\int_{t_o}^{t_n} (q_\infty/\mu_o)\,\mathrm{d}t$$

cancels out leaving only

$$\int_{t_n}^{t_{n+1}} (q_\infty/\mu_o)\,\mathrm{d}t = (2n_o/\lambda)\cos(\theta_r)(\Delta s_{n+1} - \Delta s_n)/C_f$$

This eliminates the effects of the early portion of the run and avoids the need to assume that the oil is infinitely thick (and $\Delta s = 0$) at time 0.

Practical issues impede the use of the technique in production facilities. For one, illuminating the model is a challenge—it is difficult to provide a sufficiently expansive (also known as extended) light source that can illuminate the model from all directions in the interest of imaging the fringes at every point on the model. Also, interferometry requires that specular reflections (of sufficiently coherent light) from both the air–oil interface and the model surface arrive at the observer simultaneously, allowing interference to take place at the observer. For this to occur, light viewed by the observer or camera, that specularly reflects off the model, must originate from a specific location in the test section. At another location on the model, the light that specularly reflects off the model usually originates from a different location in the test section. The model is effectively a mirror, and the image seen in the mirror gives an indication of where the light originated. Curved models are particularly problematic because light needs to originate from a very wide range of locations. Driver [3] overcame this problem by illuminating the wind-tunnel walls and letting the broadly lit walls illuminate the model. Featureless wind-tunnel walls prove to be the best reflector, whereas windows prove to be problematic.

Wind-Tunnel Setup

In a recent test in the NASA Ames 11-ft unitary plan transonic wind tunnel [10] there was a need to know the transition location on a pair of two-dimensional laminar flow airfoils. Because laminar flow was important to the performance of the airfoil, it became useful to measure the transition location in an effort to understand the lift and drag measurements. However, any dedication of time to oil-film interferometry (typically 1 h per run) would mean that fewer drag polars would be obtained in the finite period of time allocated for testing (two weeks). As a result we devised a method of acquiring data at the same time that force balance data were being acquired, thus minimizing the impact on the run schedule.

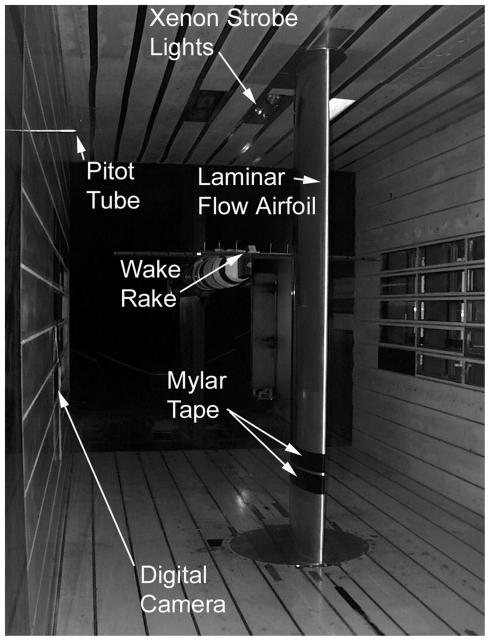

Fig. 3 Airfoil installed in NASA Ames 11-ft transonic wind tunnel.

A 2-D airfoil was installed in the NASA Ames 11-ft transonic wind tunnel (see Fig. 3). The airfoil had a 0.91 m chord and it spanned the wind tunnel from floor to ceiling. Black strips of Mylar [11] (∼0.1 mm thin) were adhered to the model at the 25% span location for the purpose of providing a partially reflective surface on which oil would be applied.

Measurements were obtained on the suction side of the airfoil using a Haselblad camera with a monochrome 4096×4096 Dicomed, Inc., digital back. The camera was installed behind a window in the wall opposite the Mylar strips. The camera was fitted with a dichroic narrow bandpass filter whose wavelength was centered on the 546 nm light emitted by the xenon flash lamps mounted in the ceiling of the wind tunnel. The flash units were aimed at the wall of the wind tunnel opposite the wing where the Mylar was mounted. The Mylar was illuminated by the diffuse reflection of the xenon flash lamps hitting the wind-tunnel wall. Direct illumination of the Mylar strip by the xenon flash lamps was undesirable and avoided. See [3] for a further explanation of why this is important.

The digital camera and the flash lamps were mounted in the pressurized environment of the wind tunnel. The camera and flash lamps were controlled remotely by a PC which also acquired wind-tunnel flow conditions such as dynamic pressure and temperature.

Just before sealing up the wind tunnel and starting the fans, silicon oil [12] is applied, in discrete patches or lines, to the Mylar surface. During running of the wind tunnel, images are acquired by the camera, downloaded to the PC, and viewed in real time (see Fig. 4). It was useful to see the images in real time to ensure optimum fringe spacing—a compromise between large fringe spacing for analysis, but close enough spacing to allow for further development at the next test point.

Pictures are acquired throughout the run. In particular, it is useful to obtain a picture at a point in time just after the tunnel achieves the desired test condition ($t = 310$ s) (see Fig. 4a). This may require waiting a minute or two so that fringes are visible in the first picture. At some time later (typically 5 min) a second picture is acquired, which records the degree to which the oil has flowed while the tunnel is running at the desired test condition (see Fig. 4b). At this point the airfoil is commanded to go to another angle of attack and a picture is acquired after another 5 or so minutes of running (see Fig. 4c). The measured oil thickness (determined from fringe spacing) at time $t = 630$ s serves as the initial condition in analyzing the fringe spacing for the image acquired at time $t = 920$ s.

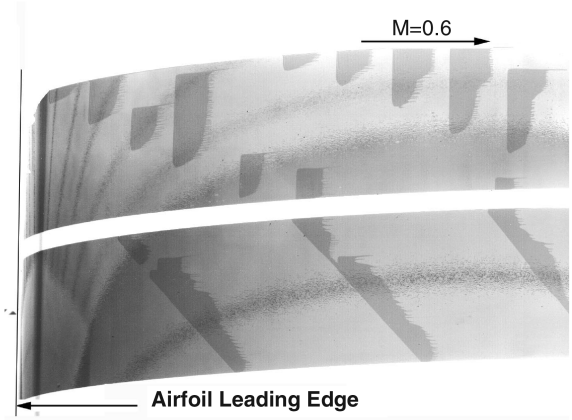

a) Time t = 310 s

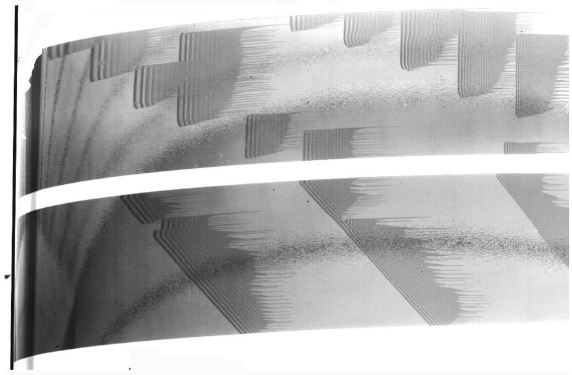

b) Time t = 630 s

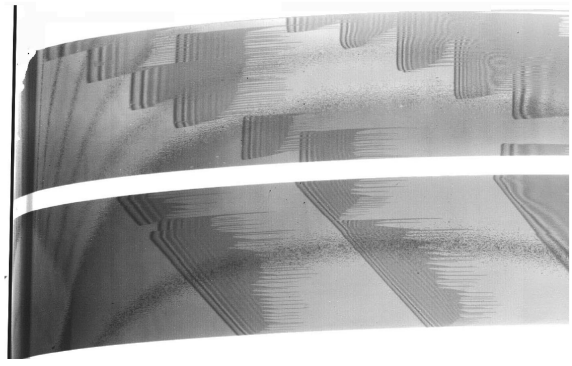

c) Time t = 920 s

Fig. 4 Images of airfoil leading edge (suction side) acquired at ~5 min intervals during a tunnel run at $M = 0.6$, $\alpha = 1$ deg, and $Re_c = 4.5 \times 10^6$, airfoil A.

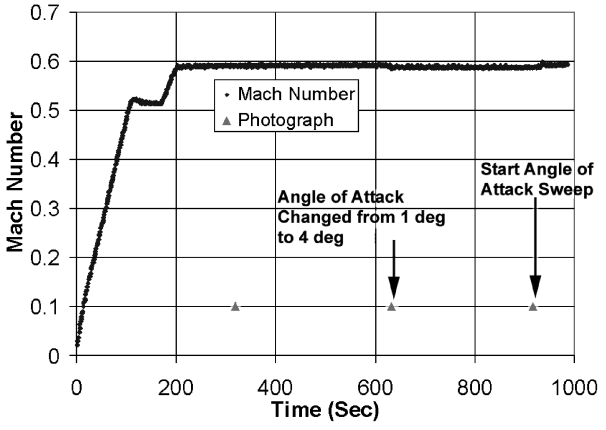

Fig. 5 Time history of tunnel Mach number and photograph acquisition.

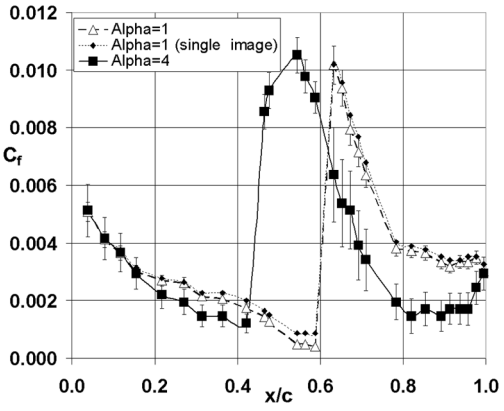

Fig. 6 Skin-friction results obtained at two angles of attack ($a = 1$ deg and $a = 4$ deg), $M = 0.6$, $Re_c = 4.5 \times 10^6$, airfoil A.

Interference patterns (called fringes) are seen within each of the oil patches shown in Fig. 4. The spacing between "fringes" is generally proportional to the skin friction except in Fig. 4c where the cumulative oil flow is a result of two test conditions. Here the skin friction is proportional to the difference in fringe spacing between the images in Figs. 4b and 4c, as calculated by Eq. (2).

During the run up of the wind tunnel, the oil flows at conditions other than the desired test condition (see Fig. 5). To eliminate the undesirable effect of the tunnel starting transient on the oil, a picture is taken at the time the tunnel first achieves the desired test condition, in this case 310 s after tunnel start. The difference of fringe spacing between this picture and the subsequent picture (at time 630 s) is used to determine the skin friction.

The process of sitting on the condition, taking a picture, and changing the angle of attack could go on indefinitely, if it were not for the oil being depleted. Practically, only two test conditions per run were possible before the oil had to be reapplied to the model. After the third picture, the airfoil was put through the usual angle of attack sweeps associated with performance testing. Typically, several hours of force measurements were obtained before the tunnel was open again and oil reapplied. Nevertheless using this approach produces two measurement sets of skin friction (as will be described in subsequent sections) at the cost of only 10 min of tunnel run time. The skin-friction measurements proved helpful in explaining abrupt changes in the drag polars obtained, in this case, by a wake rake.

Image Analysis

Skin friction can be determined from the images shown in Fig. 4. From the images the spacing between interference bands of light and dark (known as the fringe spacing) is measured often with the aid of Photoshop® or software designed for measuring features on images [13]. The spacing between the fringes Δs is related to the skin friction by Eq. (2).

Figure 6 shows the skin-friction levels obtained from processing the images seen in Fig. 4. The primary contribution to the overall uncertainty in C_f is due to uncertainty in measuring the fringe spacing ($\mathrm{d}\Delta s \sim \pm 0.07\Delta s$), and this produces an uncertainty in skin friction of

$$\Delta C_f = \pm \frac{(2n_o/\lambda)\cos(\theta_r)\sqrt{\mathrm{d}\Delta s_{n+1}^2 + \mathrm{d}\Delta s_n^2}}{\int_{t_n}^{t_{n+1}} (q_\infty/\mu_o)\,\mathrm{d}t}$$

which is represented by the error bars in Fig. 6. Uncertainties in the skin friction for the second condition are higher than for that of the first condition, especially for $x/c > 0.6$. Here the fringe spacing in each image is large relative to the difference in fringe spacing. The uncertainty is least when $\Delta s_{n+1} \gg \Delta s_n$.

Temperature of the airfoil (and thus the oil) was measured throughout the run with a resistive temperature device (RTD) sensor attached at the trailing edge near the root of the airfoil. The

temperature was used to determine the oil's viscosity. The oil's viscosity was calibrated to $\pm 1\%$ accuracy using a viscometer.

The viewing angle is to some extent nonorthogonal to the model surface (especially in the vicinity of the wing leading edge). There was no attempt to correct (via photogrammetry) for this, and θ_r was assumed to be zero for the analysis shown here.

In many experiments (where optical access is limited) it is only possible to obtain one image after the run. In Fig. 6, the skin friction was determined (for $\alpha = 1$ deg) using only the intermediate image (at $t = 630$ s) and assuming $\Delta s_n = 0$ at time $t = 0$ (shown as small solid circles). Fortunately, calculating the skin friction this way yields nearly identical results to computing skin friction by taking the difference of two images. Taking the difference of two images makes it possible to remove the effects of startup transients experienced by the oil while the tunnel is speeding up to the desired test condition. From Fig. 6 it is apparent that two conditions can be obtained during a single run, and useful information about the boundary layer state can be learned from each measurement.

Reversed Flow

In most runs, reversed flow could be detected by virtue of fringes forming at the downstream end of the oil. This situation is handled by Eq. (2). However, there are some situations where the surface shear changes direction midway through the run. This occurred in a later run in the trailing edge region of the airfoil ($x/c = 0.81$) as the angle of attack of the airfoil changed from $\alpha = 4$ deg to $\alpha = 6$ deg. While the airfoil was at 4 deg, the trailing edge flow was attached, however, when the airfoil was pitched to 6 deg later in the run, and the trailing edge region produced reversed flow. This produced an interesting time variation of the fringe spacing (see Fig. 7).

In Fig. 7, the fringes are initially growing with time and reach a maximum fringe spacing at $t = 310$ s into the run. At time $t = 310$ s the wing is pitched from $\alpha = 4$ deg to $\alpha = 6$ deg and the shear at the $x/c = 0.81$ location appears to reverse sign as evidenced by the fringe spacing diminishing with time.

To the best of our knowledge this is the first time that fringe spacing has been seen to diminish with time. To better understand the effects on the oil of reversing the direction of the shear stress in midrun, we performed a bench test where a known shear was applied to the oil. A channel with fully developed flow was used to produce a steady shear on a test sample of oil. After a period of time (25 s) the channel flow was abruptly shut off, and the plate containing the partially flowed oil film was removed and rotated 180 deg and reinstalled in the channel flow facility. Reversing the orientation of the oil flow (so that the trailing edge of the oil was now facing into the airstream) simulated reversing the direction of the shear. Video of the oil flow was acquired and selected frames are shown in Fig. 8.

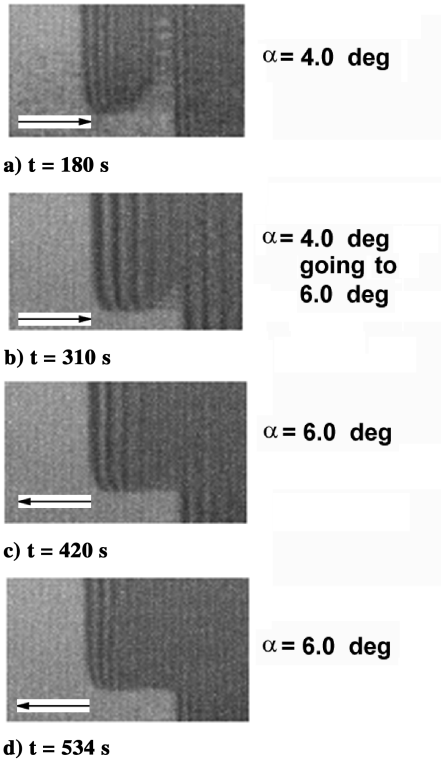

Fig. 7 Time evolution of fringe pattern at $x/c = 0.81$. Wing leading edge on left.

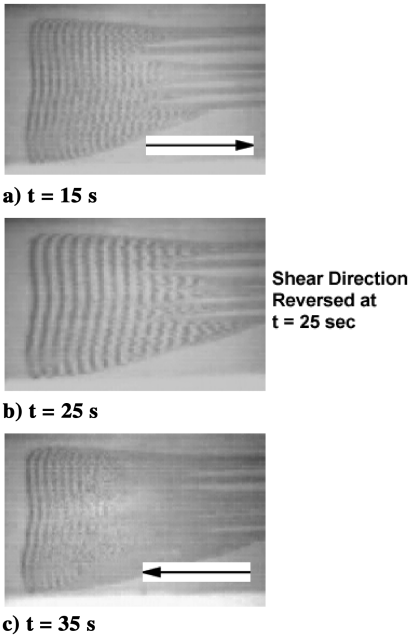

Fig. 8 Time evolution of fringe pattern in a channel flow facility.

As expected, the oil thinned with time producing increasingly larger fringe spacing until an elapsed time of 25 s. At 25 s, the flow direction (relative to the oil film) was reversed and the fringe spacing steadily decreased thereafter. Interestingly, at 35 s, the fringe spacing returned to spacing seen at 15 s. Figure 9 shows the fringe spacing as a function of time.

The rate of increase of the fringe spacing at times $t < 25$ s is equal and opposite to the rate of decrease of the fringe spacing at time $t > 25$ s. Note that the shear stress acting on the oil is equal and opposite in direction.

This linear behavior is consistent with the nature of the thin film equation that is a first-order partial differential equation with 1-D solutions of fringe spacing that are linear in time and shear. This reversal in the oil-film behavior can be shown by means of the thin film equation result [Eq. (2)] rearranged to the following form:

$$\Delta s_{n+1} - \Delta s_n = (t_{n+1} - t_n)\frac{q_\infty}{\mu_o}\frac{\lambda C_f}{2n\cos(\theta_r)}$$

where conditions are assumed constant over the time period

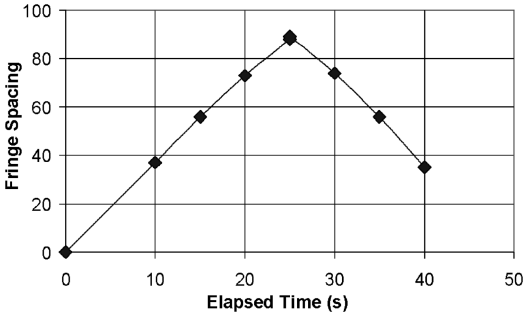

Fig. 9 Fringe spacing as a function of time. Shear direction reversed at time $t = 25$ s.

$\Delta t = (t_{n+1} - t_n)$. A change in fringe spacing $(\Delta s_{n+1} - \Delta s_n)$ is linear in time and when C_f becomes negative so does the change in fringe spacing. These results validate the use of Eq. (2) for situations where the direction of the shear reverses in midrun. To compute the shear it is necessary to measure the change of fringe spacing (requires at least two images separated in time, $t_{n+1} - t_n$) and insert that change into Eq. (2). Because ΔS_{n+1} is less than ΔS_n the resulting C_f will appropriately be negative.

Results

Transition location on laminar flow airfoils is sensitive to many things, such as Reynolds number, airfoil surface finish, and freestream disturbances to mention a few.

Reynolds Number Effects

Decreasing Reynolds number to $Re_c = 2.3 \times 10^6$ produces a more aft transition location (see Fig. 10) compared to the transition location seen for $Re_c = 4.5 \times 10^6$ (Fig. 6) in the case of airfoil A.

Comparing the skin-friction distribution for the high and low Reynolds number cases (Fig. 11) at an angle of attack $\alpha = 1$ deg shows that the C_f is very similar for the two cases.

At low Reynolds number, the flow has developed a small separation bubble that does not exist at high Reynolds number. It would appear that the low Reynolds number case develops somewhat higher skin-friction levels over the first half of the airfoil compared to the high Reynolds number case. Inherently, boundary layers grow at a faster rate when C_f is large (i.e., $d\theta/dx = -C_f$ for $dP/dx \ll 1$), where θ is the momentum thickness. A thick boundary layer is more prone to separate than a thin boundary layer, in the face of an adverse pressure gradient. In the low Reynolds number case, the separation bubble transitions to turbulence abruptly and the flow is firmly attached thereafter. Within the laminar separation bubble the flow will experience a destabilizing inflection point in the boundary layer velocity profile causing disturbances to be amplified rapidly, triggering transition to turbulence and subsequent reattachment [14]. Downstream of reattachment, the flow is relatively firmly attached as is indicated by the higher level of skin friction.

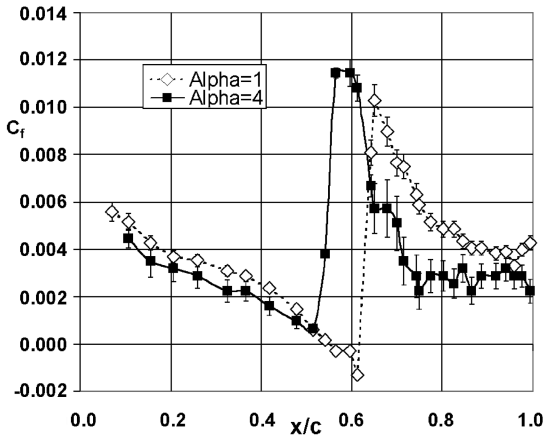

Fig. 10 Skin-friction distribution for airfoil A obtained at two angles of attack ($\alpha = 1$ deg and $\alpha = 4$ deg), $M = 0.6$, $Re_c = 2.3 \times 10^6$.

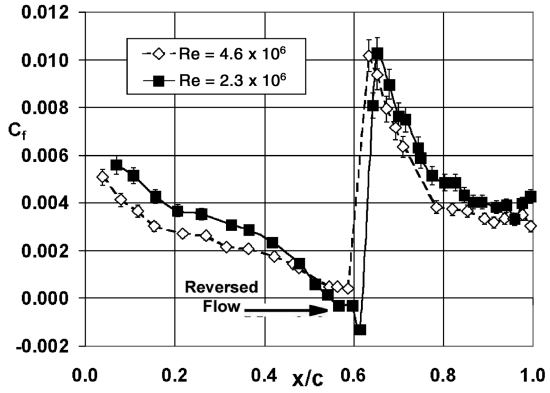

Fig. 11 Skin-friction distribution for airfoil A, at $M = 0.6$, $\alpha = 1$ deg at two different Reynolds numbers.

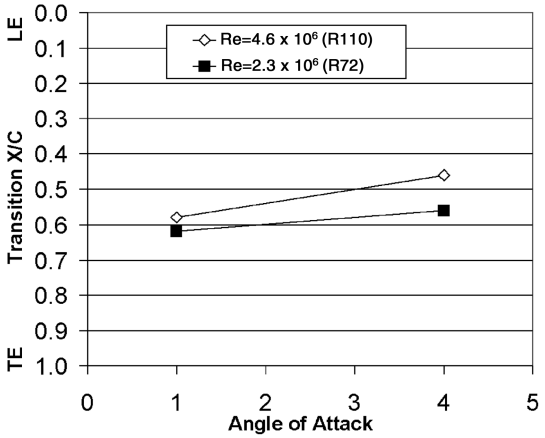

Fig. 12 Transition location as a function of Reynolds number and α at $M = 0.6$, airfoil A.

The somewhat earlier transition in the case of high Reynolds number is probably caused by the higher momentum thickness Reynolds number, Re_θ, and the higher associated amplification rate of disturbances. The effects of Reynolds number on transition are summarized in Fig. 12. Increasing the Reynolds number from 2.3×10^6 to 4.6×10^6 promotes earlier transition as can be seen in Fig. 12. However the effect of Reynolds number is not nearly as dramatic as is the effect of disturbances as will be seen in the following sections.

Trip Wire Induced Transition

The performance of laminar flow airfoils typically deteriorates as the transition location moves forward. To test this theory, we introduced a 0.5 mm diam trip wire at $x/c = 0.45$. We compared skin-friction distributions with and without the trip wire (see Fig. 13).

Note that the measurements shown in Fig. 13 are for a different airfoil than the data shown in the previous figures. Although there are slight differences between the two airfoils, the trends in skin friction are similar.

In the case of natural transition, the flow produces a small laminar separation bubble at $x/c = 0.65$ which abruptly transitions to turbulence as it reattaches. In the case of the trip wire, the boundary layer transitions to turbulence immediately downstream of the wire. Soon after the trip, the levels of skin friction are significantly higher than for that of the naturally transitioning boundary layer. These high

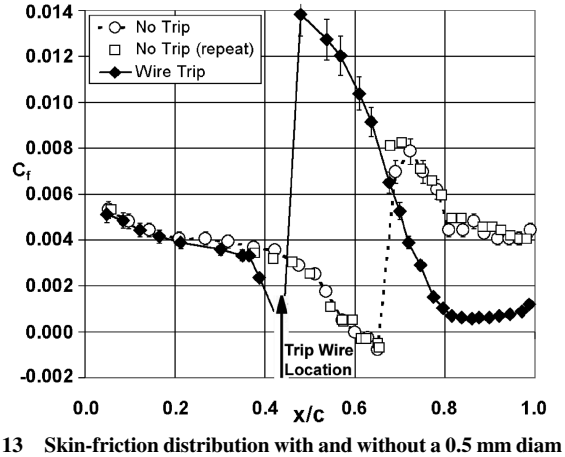

Fig. 13 Skin-friction distribution with and without a 0.5 mm diam trip wire ($x/c = 0.45$) obtained for airfoil B at $M = 0.6$, $\alpha = 1$ deg, and $Re_c = 2.3 \times 10^6$.

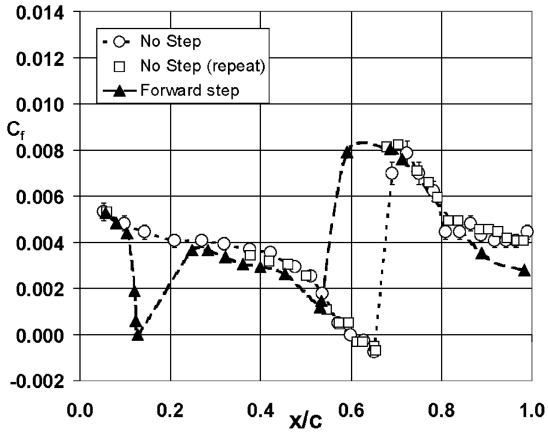

Fig. 14 Skin-friction distribution with and without a 0.4 mm high forward-facing step ($x/c = 0.13$), airfoil B at $M = 0.6$, $\alpha = 1$ deg, and $Re_c = 2.3 \times 10^6$.

levels of shear will likely cause the boundary layer to grow more rapidly than the naturally transitioning boundary layer. Downstream, the tripped boundary layer becomes lethargic (low levels of shear), verging on separation, as it travels through the adverse pressure gradient, $0.5 < x/c < 1.0$. This leads to a thicker boundary layer and less trailing edge pressure recovery.

Forward-Facing Step Disturbance

A forward-facing step (a 0.4 mm high strip of plastic) disturbance was incorporated onto the model at $x/c = 0.13$. The plastic strip had a wedge-shaped cross section so that the thick end of the strip was upstream and the thin end was downstream. The plastic strip tapered to near zero at the downstream end of the wedge so as to minimize the disturbance there. Skin friction was measured and shown in Fig. 14.

Interestingly, the flow does not immediately transition to turbulence at the forward-facing step. In fact it does not transition until 50% chord, not much ahead of natural transition. Remarkably the skin friction downstream of transition is not much different than the natural transition case. In contrast, the 0.5 mm trip wire transitions the flow almost immediately downstream of the wire. Apparently, a forward-facing step produces less of a disturbance than slightly larger trip wire.

Leading Edge Disturbance

A roughness element on the leading edge of airfoil B was discovered during a skin-friction run. During the first portion of the run, the angle of attack was set at $\alpha = 1$ deg and the fringes produced (see Fig. 15a) were typical of other runs. After changing the angle of attack to $\alpha = 4$ deg, the fringes became distorted, indicating a local disturbance (see Fig. 15b).

The width of the disturbance was seen to grow with downstream distance, leaving a wake that was growing like a wedge. At the vertex of the wedge-shaped wake we found a 0.1 mm tall and 0.25 mm diam burr on the leading edge of the airfoil (remnants of machining). A turbulent wedge had formed downstream of the burr in the case of $\alpha = 4$ deg (see Fig. 15b); however, the burr did not trigger turbulence in the case of $\alpha = 1$ deg (see Fig. 15a). This is an indication of the sensitive nature of transition and the need to keep the leading edge of laminar flow airfoils disturbance free. The skin friction associated with this run is shown in Fig. 16.

The undisturbed portion of the airfoil produces a shear distribution that is similar to airfoil A. However, downstream of the burr the shear distribution (triangles) produces high levels of shear in the upstream region of the flow, followed by a rapid reduction to near zero shear in the trailing edge region of the flow. This behavior is very similar to that of the trip wire case, albeit at different angles of attack. This highlights the sensitive nature of this laminar flow airfoil to small imperfections in manufacturing and roughness such as might occur during flight from impacts, dirt, and bugs.

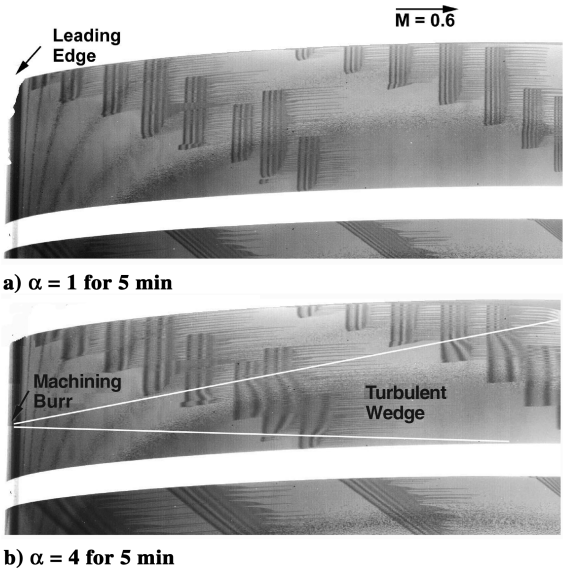

Fig. 15 Images of airfoil B leading edge at 5 min intervals, $M = 0.6$, $\alpha = 1$ deg, and $Re_c = 2.3 \times 10^6$.

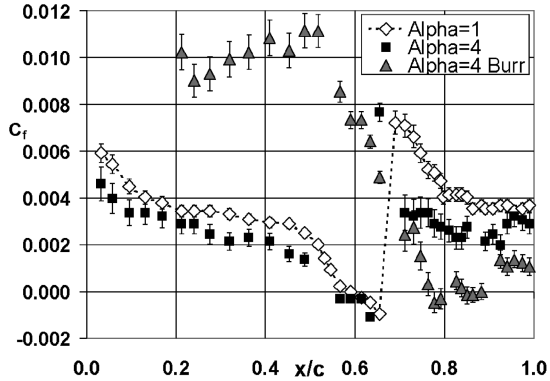

Fig. 16 Skin-friction distribution on airfoil B at $M = 0.6$ and $Re_c = 2.3 \times 10^6$ for angles of attack $\alpha = 1$ deg and $\alpha = 4$ deg.

Conclusions

Improvements to the oil-film interferometry technique have enabled multiple sets of skin-friction measurements to be obtained in a production wind tunnel for the first time. Tests on a laminar flow airfoil in the NASA Ames 11-ft transonic wind tunnel demonstrate the ability to acquire skin-friction measurements with a minimal impact on tunnel run time. Two conditions were acquired per run; this more than doubles the productivity seen in previous studies. Furthermore, by virtue of the unique lighting scheme, it is possible to take pictures during production tunnel runs, rather than shutting down and taking pictures. Not shutting down allowed us to obtain two skin-friction distributions during runs that were otherwise dedicated to force measurements.

For the first time, fringes were seen to decrease in spacing with time. During particular tests the fringe spacing was seen to get smaller with time after a change of model conditions. This behavior was attributed to reversed flow. A bench-top experiment determined that the same equation used to calculate shear stress for fringes that are growing could be used to calculate she shear stress for fringes that are contracting with time.

Laminar flow was seen as far back as 60% chord at a Reynolds number (based on chord) of 4.5×10^6. In some cases transition occurred within a small laminar separation bubble. Several disturbances introduced on the airfoil surface promoted transition to turbulence upstream of the naturally occurring transition point. In the cases with a trip wire disturbance and a machining burr disturbance, the shear level downstream of the disturbance was initially high

followed by a steady decline to near zero in the vicinity of the trailing edge, far below the level of shear for the naturally occurring transition. These results point out the sensitive nature of laminar flow airfoils to small disturbances.

References

[1] Mateer, G. G., Monson, D. J., and Menter, F. R., "Skin-Friction Measurements and Calculations on a Lifting Airfoil," *AIAA Journal*, Vol. 34, No. 2, 1996, pp. 231–236.
doi: 10.2514/3.13055

[2] Drake, A., and Kennelly, R. A., Jr., "Oil Film Interferometry for Skin Friction Measurement on an Aircraft in Flight," *Journal of Aircraft*, Vol. 36, No. 4, 1999, pp. 723–725.
doi: 10.2514/2.2498

[3] Driver, D. M., "Application of Oil-Film Interferometry Skin-Friction Measurements to Large Wind Tunnels," *Experiments in Fluids*, Vol. 34, No. 6, June 2003, pp. 717–725.
doi: 10.1007/s00348-003-0613-1

[4] Wadcock, A. J., Yamauchi, G. K., and Driver, D. M., "Skin Friction Measurements on a Rotor in Hover," *Journal of the American Helicopter Society*, Vol. 44, No. 4, Oct. 1999, pp. 312–319.

[5] Kennelly, R. A., Jr., Westphal, R. V., Mateer, G. G., and Seelen, J., "Surface Oil Film Interferometry on a Swept Wing Model in Supersonic Flow," *Flow Visualization VII, Proceedings of the 7th International Symposium on Flow Visualization*, edited by J. P. Crowder, Begell House, New York, Sept. 1995, pp. 302–307.

[6] Tanner, L. H., and Blows, L. G., "A Study of the Motion of Oil Films on Surfaces in Air Flow, with Application to the Measurement of Skin Friction," *Journal of Physics E: Scientific Instruments*, Vol. 9, No. 3, March 1976, pp. 194–202.
doi: 10.1088/0022-3735/9/3/015

[7] Monson, D. J., Mateer, G. G., and Menter, F. R., "Boundary-Layer Transition and Global Skin Friction Measurement with an Oil-Fringe Imaging Technique," SAE Paper 932550, Sept. 1993.

[8] Squire, L. C., "Flow Visualization in Wind Tunnels Using Indicators," AGARDograph 70, edited by R. L. Maltby, April 1962, pp. 7–55.

[9] Brown, J. L., and Naughton, J. W., "The Thin Oil Film Equation," NASA TM 1999-208767, March 1999.

[10] Baals, D. D., and Corliss, W. R., "Wind Tunnels of NASA," NASA SP-440, 1981.

[11] MonoKote, Top Flite Models, Inc., Champaign, IL.

[12] Information About Dow Corning Silicone Fluids, Dow Corning Corp., Midland, MI, 1994.

[13] Zilliac, G. G., "The Fringe-Imaging Skin Friction Technique PC Application User's Manual," NASA TM 1999-208794, Sept. 1999.

[14] Dini, P., Selig, M. S., and Maughmer, M. D., "Simplified Linear Stability Transition Prediction Method for Separated Boundary Layers," *AIAA Journal*, Vol. 30, No. 8, Aug. 1992, pp. 1953–1961.
doi: 10.2514/3.11165

R. Lucht
Associate Editor